American Mineralogist, Volume 75, pages 529–538, 1990

Ion exchange reactions between dehydroxylated micas and salt melts and the crystal chemistry of the interlayer cation in micas

HANS KEPPLER*
Mineralogisches Institut der Universität, Kaiserstraße 12, 7500 Karlsruhe, Federal Republic of Germany

ABSTRACT

The interlayer cations in dehydroxylated micas can be exchanged by reaction with salt melts (chlorides and bromides) at temperatures of 700 to 950 °C under atmospheric pressure within a few hours. Generally, during the reactions air and moisture must be excluded to prevent decomposition of the micas. By this method, dehydroxylated mica phases of the type $M^{+}Al_2[AlSi_3O_{10}O]$ with M = Li, Na, K, Rb, Cs, Tl were prepared as well as micas of the type $M_{½}\square_{½}Al_2[AlSi_3O_{10}O]$ with M = Ca, Sr, Ba. Additionally, a sodium mica was prepared with part of the Na^{+} ions replaced by La^{3+}, probably according to the reaction $3\ Na^{+} = La^{3+} + 2\square$. Most of these micas are compounds not described previously. For all micas except the Sr and Ba phases, complete sets of lattice constants are given. The lattice constants are almost exclusively determined by the ionic radius and not by the charge of the interlayer cation. The tetrahedral rotation angle can be varied by about 10° solely by the interlayer substitution. In micas with very small interlayer cations like Na^{+} or Li^{+}, repulsive forces between the O atoms across the interlayer region cause an interlayer overshift, resulting in anomalously high basal spacings and a smaller β angle. The interlayer spacing of the lithium mica can expand by reversible uptake of water. The other dehydroxylated micas do not react with water at room temperature. The differences in the structure of micas with small and large interlayer cations explain many features of the geochemistry of these phases, such as the miscibility gap between paragonite and muscovite, the preferential uptake of potassium in micas and structurally related clay minerals, and the smaller thermodynamic stability range of paragonite compared with muscovite.

INTRODUCTION

Interlayer cations of micas are not easily exchanged, in contrast to the structurally related clay minerals. Even at high pressures and temperatures, reaction times of several weeks are necessary to reach chemical equilibrium between fine-grained micas and aqueous salt solutions (Iiyama, 1964; Scott and Smith, 1966; Krausz, 1974; Flux and Chatterjee, 1986).

White (1954) and Franz and Althaus (1976) tried to exchange the interlayer cations of micas by reaction with salt melts. White obtained only decomposition products. Franz and Althaus were able to partially replace the K in phengites by Na, but some decomposition of the micas to other phases was always observed. Fujii (1966) obtained solid solutions between dehydroxylated paragonite and dehydroxylated muscovite by ion exchange between salt melts and muscovite. During the experiments, part of the mica reacted to nepheline, hydroxysodalite, and other phases.

In this paper, ion-exchange reactions between water-free, dehydroxylated micas and salt melts are described that allow the introduction of a wide variety of cations into the interlayer of micas (cf. Keppler, 1988). During these reactions, the mica structure is completely preserved and no decomposition occurs. The reaction products are used to study the influence of the interlayer substitution on the crystal structure of these phases.

EXPERIMENTAL METHODS

Starting materials

Paragonite-$2M_1$ and muscovite-$2M_1$ were prepared by hydrothermal treatment of stoichiometric mixtures of amorphous SiO_2 (spec. pure), chemically pure $Al(OH)_3$, and 4N solutions of NaOH or KOH at 7 kbar for 14 days. The reaction temperature was 550 to 600 °C for paragonite and 650 to 700 °C for muscovite. X-ray diffraction patterns indicate the presence of small amounts of the 1M polytype in the paragonite samples, but no other impurities were detected. The diffraction patterns are similiar to those given by Chatterjee (1970) and Chatterjee and Johannes (1974). According to SEM investigations, the samples consist of aggregates of irregularly shaped platelets ranging from 1 to 5 μm in size. Dehydroxylated paragonite and muscovite were prepared by heating the corresponding mica at 850 °C for 5 h. IR spectra showed that the products obtained were completely water-free.

* Present address: Bayerisches Geoinstitut, Universität Bayreuth, Postfach 101251, Universitätsstraße 30, 8580 Bayreuth, Federal Republic of Germany.

0003–004X/90/0506–0529$02.00

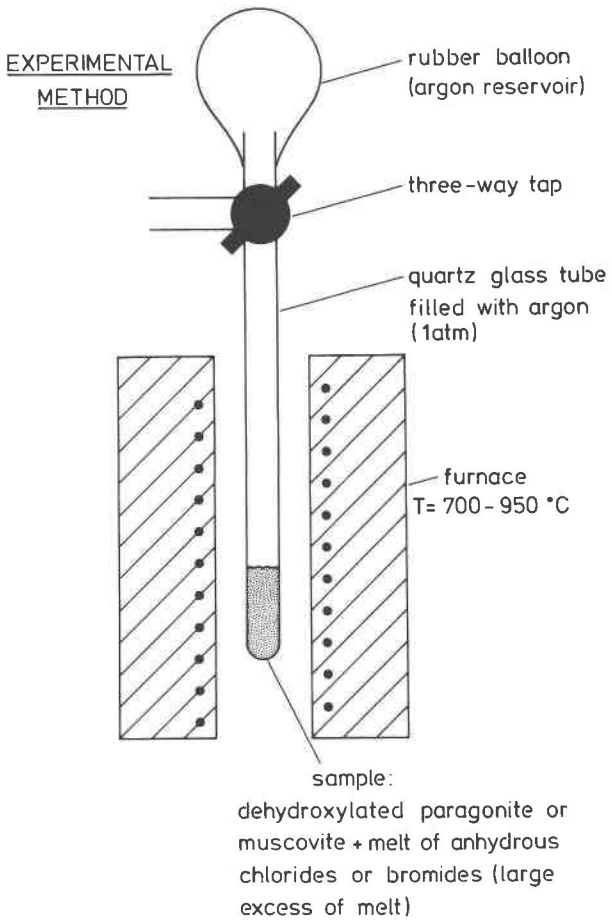

Fig. 1. Experimental scheme used for performing ion-exchange reactions in an inert-gas atmosphere.

Ion exchange between micas and salt melts

The interlayer cations in dehydroxylated muscovite-$2M_1$ or paragonite-$2M_1$ were exchanged by reaction with melts of anhydrous chlorides or bromides at 700 to 950 °C under atmospheric pressure within a few hours. Both dehydroxylated paragonite and dehydroxylated muscovite can be used as starting materials for all reactions. To facilitate X-ray identification of reaction products, the mica that was expected to show the greater change of lattice constants after the ion exchange was usually chosen.

The exchange reactions between micas and KCl, RbCl, and CsCl were performed in a Pt crucible in air using an electric furnace. In these cases, both hydroxyl-containing and dehydroxylated micas could be used as starting materials. In all other cases, however, it was necessary to exclude moisture and oxygen by working in an inert gas atmosphere and to use absolutely water-free starting materials (dehydroxylated micas and anhydrous salts). Otherwise, reactions between the salt melt and H_2O or O_2 would occur that would lead to the formation of strongly alkaline substances (e.g., CaO and LiOH), according to equations of the type $2\ CaCl_2 + O_2 \rightarrow 2\ CaO + 2\ Cl_2$ or $LiCl + H_2O \rightarrow LiOH + HCl$ (Gmelin 1927, 1957). These alkaline compounds would attack the silicate framework of the mica and lead to decomposition. Reactions under inert gas were performed in a quartz-glass tube filled with argon (Fig. 1).

A high excess of salt melt compared to the amount of mica was always used in order to obtain an almost complete cation exchange. After the run, the excess of salt was dissolved away with water (for NaCl, KCl, RbCl, CsCl), very dilute aqueous HCl ($CaCl_2$, $SrCl_2$, $BaCl_2$, $BaBr_2$, $LaCl_3$), aqueous solution of sodium thiosulfate (TlBr), or absolute ethanol (LiCl).

Investigation of reaction products

Chemical analyses. Quantitative analyses were performed by means of atomic absorption spectrometry after dissolving the samples in $HF + HClO_4$. SiO_2 was determined by difference, with the sum of all oxides being 100 wt%. Analyses of the reaction products by electron microprobe gave only semiquantitative results because the small grain size and perfect cleavage of the micas made the preparation of polished surfaces impossible.

IR spectra. Pellets were prepared by pressing a mixture of 1–2 mg of sample and 200–300 mg of KBr. After heating in a vacuum at 200 °C for several hours to remove adsorbed water, the IR spectra of the samples were measured using a Beckman spectrometer IR 4250.

X-ray diffraction. X-ray diffraction patterns of powder samples were obtained by means of a Philips diffractometer PW 1050/25 (proportional counter, Ni-filtered Cu$K\alpha$ radiation, scan rate ⅛° 2θ/min, time constant 2 s, 5–70° 2θ, internal standard of high-purity silicon). Lattice constants based on the powder data were refined by a least-squares procedure.

Experimental results and discussion

Synthesis of mica phases by ion exchange

The conditions for the synthesis of the mica phases described in this paper are summarized in Table 1. The reaction products are fine-grained white powders that are soft to the touch. Figure 2 shows the X-ray diffraction pattern of the product obtained by ion exchange between dehydroxylated paragonite and KCl melt. The pattern is virtually identical with that of dehydroxylated muscovite. The substitution of alkalies (and thallium) in the interlayer causes a significant shift of the (002) basal reflection (Fig. 3). The products of the ion exchange with halogenides of calcium, strontium, and barium do not show a strong (002) basal reflection. However, (006) always has high intensity in the diffraction patterns, and its position strongly depends on the size of the interlayer cation (Fig. 4). Table 2 gives the chemical analyses of three alkali micas prepared by ion exchange between alkali halogenide melts and dehydroxylated paragonite. The measured compositions are almost identical with the calculated composition of dioctahedral potassium, rubid-

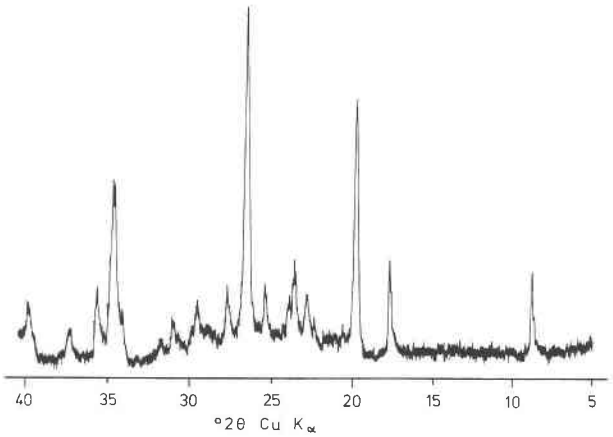

Fig. 2. X-ray diffraction pattern of potassium mica prepared by ion exchange between dehydroxylated paragonite and KCl melt. The pattern is virtually identical with that of dehydroxylated muscovite.

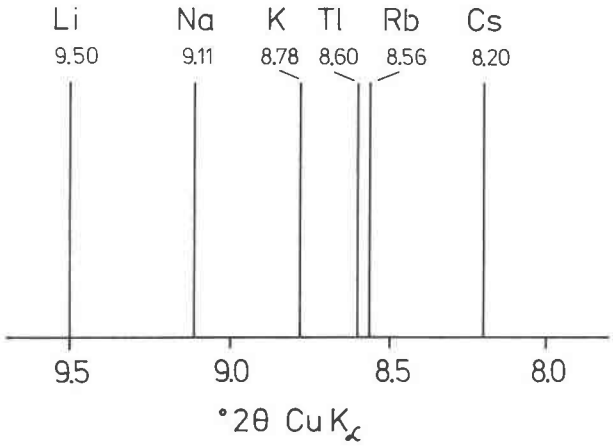

Fig. 3. Position of the (002) basal reflection of dehydroxylated dioctahedral micas with univalent interlayer cations. The value for Rb is calculated from the lattice parameters because the reflection has low intensity and is difficult to measure.

ium, and cesium micas. This confirms the stoichiometric nature of the ion exchange process. Samples of the rubidium and cesium mica were treated with a large excess of NaCl at 850 °C for 2 h. Dehydroxylated paragonite was obtained as a reaction product, demonstrating the reversibility of the reaction. The IR spectra of the dehydroxylated paragonite used as starting material and the cesium mica obtained by ion exchange are compared in Figure 5. Aside from small frequency shifts, the spectra are almost identical, demonstrating that the silicate framework of the mica was not altered by the ion exchange. For the lithium mica, quantitative analyses cannot be given because the samples obtained always contained some decomposition products (strong X-ray reflections at 4.55 and 3.51 Å; a phase very similar to, but probably not identical with β-eucryptite, $LiAlSiO_4$). The decomposition is probably caused by the presence of some water in these experiments. The LiCl used as salt melt is extremely hygroscopic and takes up a considerable amount of water, even during the short time necessary for handling the chemical in air during the preparation of the experiments. Under absolutely water-free conditions, the pure lithium mica could probably be obtained. In the absence of quantitative chemical analyses, the chemical formula of the lithium mica given in Table 1 is based on the lattice parameters (Table 3) that correspond to a dioctahedral mica. The magnitude of b for the lithium mica is smaller than that of b of the starting material (dehydroxylated paragonite), which precludes the incorporation of Li in the vacant sites of the octahedral layer. Therefore, all Li must be in the interlayer, which is in agreement with the very low value of c (Table 3) and leads to the formula given in Table 1. The calcium, strontium, and barium mica samples usually contained a small amount of unreacted starting material. The microprobe data confirm that the Al-Si ratio of these samples was not changed by the ion exchange process, indicating an unchanged composition of the tetrahedral and octahedral layer. To maintain charge balance, the interlayer of these micas must contain vacancies, as indicated in the chemical formulas given in Table 1. If the charge balance were achieved by substitution of Al for Si in the tetrahedral layer, the total Al-Si ratio of the mica would have to change from 1:1 to 2:1. Although the microprobe data are only semiquantitative, they clearly rule out this possibility. An analogous substitution mechanism with vacancies in the interlayer probably accounts for the incorporation of a small amount of lanthanum (La^{3+}) into the mica phase when it is treated with a NaCl-$LaCl_3$ melt (Table 1). Treatment of dehydroxylated paragonite or dehydroxylated muscovite with pure molten $LaCl_3$ yields only decomposition products.

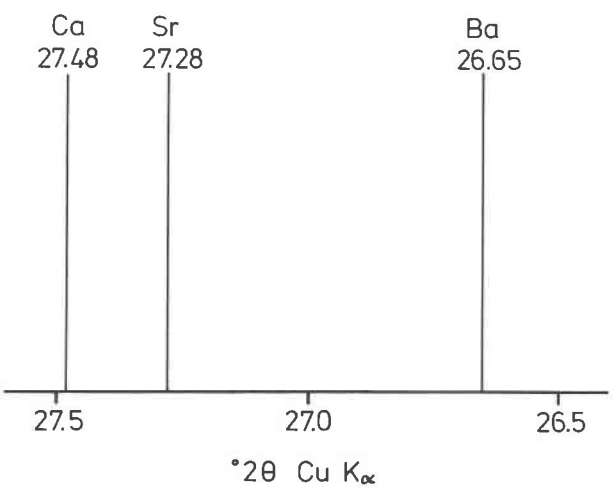

Fig. 4. Position of the (006) reflection of dehydroxylated dioctahedral micas with divalent interlayer cations.

TABLE 1. Data for synthesis of micas by ion exchange

	Starting material	Salt melt	Weight ratio salt melt to mica	Reaction temperature (°C)	Reaction time (h)	
Lithium mica						
$LiAl_2[AlSi_3O_{10}O]$	P	LiCl (under Ar)	5:1 to 10:1	700–750	1	*
Sodium mica						
$NaAl_2[AlSi_3O_{10}O]$	M	NaCl (under Ar)	100:1	900	2–5	
Potassium mica						
$KAl_2[AlSi_3O_{10}O]$	P	KCl (in air)	100:1	850	5	
Rubidium mica						
$RbAl_2[AlSi_3O_{10}O]$	P	RbCl (in air)	100:1	900	5	
Cesium mica						
$CsAl_2[AlSi_3O_{10}O]$	P	CsCl (in air)	100:1	900	5	
Thallium mica						
$TlAl_2[AlSi_3O_{10}O]$	P	TlBr (in air)	20:1	750	8	**
Calcium mica						
$Ca_{0.5}\square_{0.5}Al_2[AlSi_3O_{10}O]$	M	$CaCl_2$ (under Ar)	5:1	850	1	
Strontium mica						
$Sr_{0.5}\square_{0.5}Al_2[AlSi_3O_{10}O]$	P	$SrBr_2$ (under Ar)	10:1	850	2,5	**
Barium mica						
$Ba_{0.5}\square_{0.5}Al_2[AlSi_3O_{10}O]$	P	$BaBr_2 + BaCl_2$ (2:1) (under Ar)	10:1	950	9	**
Sodium-lanthanum mica						
Sodium mica containing 1–2 wt% La_2O_3	M	$NaCl + LaCl_3$ (9:1) (under Ar)	20:1	850	2	

Note: P = dehydroxylated paragonite, M = dehydroxylated muscovite. The composition of salt mixtures is given in weight ratios.
* Contains decomposition products.
** Product contains some unreacted starting material.

Crystal chemistry of the interlayer cation in micas

In Figure 6, the basal spacing $d(001)$ is plotted against the radius of the interlayer cation for the dehydroxylated alkali micas (compare Table 3; complete X-ray powder-diffraction data of the micas are given in Appendix 1). Surprisingly, the data points do not form a straight line; there is a jump between Na and K. The monoclinic angle β of the alkali micas exhibits a similar behavior; although it is about 96° for the potassium, rubidium, and cesium micas, it decreases to about 91° for the lithium and sodium micas. Both observations point to a fundamental difference in the coordination of the small and the large alkali ions in the interlayer. The unexpectedly high basal spacings and low values of the angle β for the small interlayer cations can be understood on the basis of the crystal structure of paragonite-$2M_1$. Because of the small size of the Na^+ ion, in the paragonite structure the O atoms forming the boundary of the interlayer region come close enough that repulsive forces result (Lin and Bailey, 1984). The difference in the coordination of the small and large alkali ions in the interlayer of a mica is schematically depicted in Figure 7. The large cations are coordinated by two sixfold rings of O atoms of the tetrahedral sheets (which appear as brackets in the cross section shown in Fig. 7). If the size of the interlayer cation is reduced, repulsive forces between the tetrahedral sheets allow an overshift of the tetrahedral layer over the interlayer cation (Lin and Bailey 1984). This causes an increased basal spacing and reduced value of β.

TABLE 2. Chemical analyses of micas prepared by ion exchange between dehydroxylated paragonite and alkali halogenide melts

	Measured wt%	Theoretical wt%
Potassium mica $KAl_2[AlSi_3O_{10}O]$		
K_2O	12.89	12.38
Na_2O	0.49	—
Al_2O_3	39.62	40.22
SiO_2	47.00	47.40
Rubidium mica $RbAl_2[AlSi_3O_{10}O]$		
Rb_2O	21.82	21.91
Na_2O	0.53	—
Al_2O_3	35.69	35.85
SiO_2	41.96	42.24
Cesium mica $CsAl_2[AlSi_3O_{10}O]$		
Cs_2O	29.07	29.72
Na_2O	0.55	—
Al_2O_3	32.41	32.26
SiO_2	37.97	38.02

Note: Total wt% = 100 because SiO_2 wt% was determined by difference.

The pseudohexagonal oxygen rings in the tetrahedral layers of micas always show some ditrigonal distortion. The amount of distortion is directly correlated to the magnitude of b according to the relation $\cos \alpha = b/b_{ideal}$ (Bailey 1984), where α is the tetrahedral rotation angle. It gives the amount by which the tetrahedra in the sixfold rings are rotated from their positions in ideal hexagonal geometry. The parameter b_{ideal} is the b lattice constant for a mica containing undistorted hexagonal rings (b_{ideal} = 9.335 Å for Al:Si = 1:3 in the tetrahedral layer, Bailey 1984). Both b and α of the alkali micas are plotted in Figure 8 as a function of the radius of the interlayer cation. Apparently it is possible to change the tetrahedral rotation angle by about 10° (from 8.96° for Cs to 18.88° for Li) solely by the interlayer substitution. This disproves earlier assumptions that the tetrahedral rotation is essentially controlled by the composition of the octa-

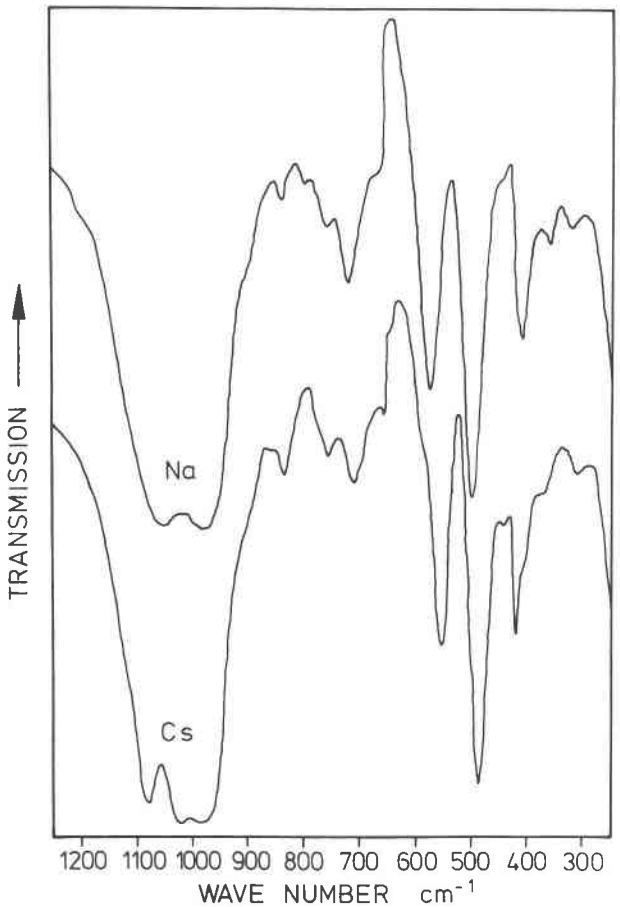

Fig. 5. IR spectra of dehydroxylated paragonite (Na) and the mica obtained by ion exchange between dehydroxylated paragonite and molten CsCl (Cs).

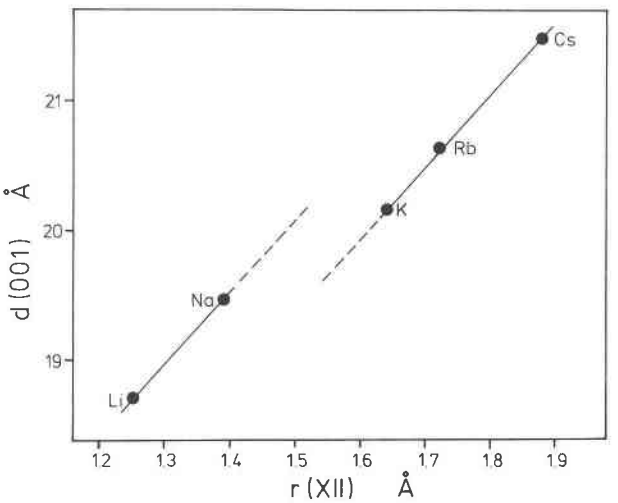

Fig. 6. Plot of the (001) basal spacing against the radius of the interlayer cation for the alkali micas. Data from Table 3.

hedral layer (McCauley and Newnham, 1971). In contrast to this idea, Radoslovich and Norrish (1962) considered the interlayer cation to be the primary control of the tetrahedral rotation angle: "For the micas in particular the surface oxygen triads rotate . . . until half of the oxygens 'lock' onto the interlayer cation." This interpretation is consistent with the experimental data presented in this paper. As in the case of $d(001)$ and β, the greatest change in b and α occurs between Na and K. This can be explained by the fact that the small interlayer cations are partially pulled out of the sixfold oxygen rings of the tetrahedral sheets (see Fig. 7), which causes a higher tetrahedral rotation angle and a correspondingly smaller value of b.

The plot of the cell volume of the alkali micas against the radius of the interlayer cation for 12-fold coordination (Fig. 9) is not a straight line. The nonlinearity is caused by the increasing tetrahedral rotation with decreasing size of the interlayer cation, leading to a distortion of the coordination polyhedron around the interlayer cation and a reduction in the effective coordination number. For that reason, the radii for 12 coordination used in Figure 9 are slightly too high for the small cations with a lower effective coordination number, explaining the deviation of the curve from a straight line. No discontinuity is observed between Na and K because the anomalously

TABLE 3. Lattice parameters, basal spacings $d(001)$, and tetrahedral rotation angles α of dehydroxylated, dioctahedral micas (monoclinic, assumed space group $C2/c$)

Interlayer cation	$^{[12]}r$ (Å)	a (Å)	b (Å)	c (Å)	β (°)	$d(001)$ (Å)	α (°)	V (Å^3)
Li	1.25	5.244(20)	8.833(22)	18.716(29)	90.50(33)	18.715	18.88	866.9
Na	1.39	5.244(08)	8.893(11)	19.463(05)	91.20(08)	19.459	17.70	907.4
K	1.64	5.225(04)	9.163(05)	20.275(05)	95.78(03)	20.172	11.02	965.8
Rb	1.72	5.243(04)	9.198(10)	20.764(06)	95.98(04)	20.652	9.83	996.0
Cs	1.88	5.263(04)	9.221(12)	21.604(08)	95.68(04)	21.498	8.96	1043.3
Tl	1.70	5.234(04)	9.177(09)	20.720(05)	95.91(04)	20.610	10.56	990.0
Ca	1.34	5.251(06)	8.891(07)	19.480(17)	91.64(12)	19.472	17.74	909.1
Sr	1.44					19.614		
Ba	1.61					20.069		

Note: The sodium and potassium micas were prepared by dehydroxylation of paragonite-2M$_1$ or muscovite-2M$_1$, respectively; the other micas were obtained by ion exchange (Table 1). Complete X-ray powder data are given in the appendix. The effective ionic radius for 12 coordination is $^{[12]}r$, according to Shannon (1976). The value for Li was calculated by linear extrapolation of the radii for lower coordination numbers.

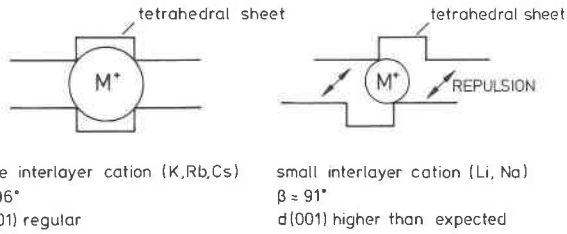

Fig. 7. Simplified model for the coordination of the interlayer cation in micas.

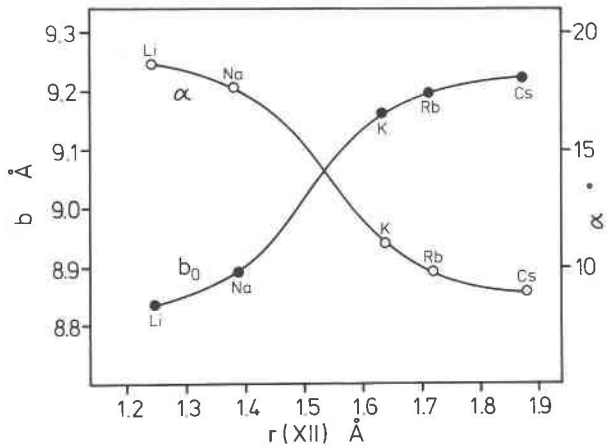

Fig. 8. Plot of b and the tetrahedral rotation angle (α) against the radius of the interlayer cation for the alkali micas.

large basal spacings and small values of b for the small cations mutually compensate in the calculation of the cell volumes.

The lithium mica exhibits a behavior which is unique among the alkali micas; its interlayer spacing can expand by a reversible uptake of water. Figure 10 shows the X-ray diffraction pattern of a sample of the lithium mica that was exposed to humid air for several days. In addition to the usual X-ray reflection at 9.5° 2θ Cu$K\alpha$, a line appears at 7.3° which corresponds to an expanded basal spacing of 12.1 Å. This reflection disappears after heating for 1 h at 700°C in a vacuum. The ability of the lithium mica to take up water can be explained by the existence of repulsive forces in the interlayer region and by the high hydration energy for Li^+ (519 kJ/mol, compared to 264 kJ/mol for Cs^+; Cotton and Wilkinson, 1980).

The size of the Tl^+ ion is almost identical to that of Rb^+ (Table 2), but Tl^+ is much more easily polarized than Rb^+ (Cotton and Wilkinson, 1980). The lattice parameters of the rubidium and thallium micas are very similar (Table 2), as expected on the basis of the ionic radii. However, a closer examination of the data shows that b of the thallium mica is significantly reduced compared to that of the Rb phase. The value of b for thallium is closer to that for K than to that of the Rb mica. It is possible that the easily polarized electron shell of the Tl^+ ion can be deformed by the oxygen atoms of the tetrahedral layer, causing an increased tetrahedral rotation angle and a reduced value of b.

The lattice parameters of the sodium and calcium micas are virtually identical, and $d(001)$ of the barium mica is very close to the value for K. Both observations demonstrate that the charge of the interlayer cation and the existence of vacancies in the interlayer have very little influence on the lattice parameters.

The influence of dehydroxylation on the mica structure

The crystal structure of dehydroxylated muscovite has been determined by Udagawa et al. (1974). The main difference from the structure of muscovite is in the coordination of Al in the octahedral sheet. Whereas Al is octahedrally coordinated by O and OH in muscovite, it is surrounded by five O atoms in trigonal-bipyramidal configuration in the dehydroxylated phase. The interlayer and the neighboring tetrahedral sheets are little affected by the dehydroxylation. Therefore, conclusions concerning the crystal chemistry of the interlayer cations in dehydroxylated micas very probably also hold for hydroxyl-containing micas. This idea is supported by results of Fujii (1966), which show that the miscibility gap between dehydroxylated paragonite and dehydroxylated muscovite is virtually identical with the two-phase region of natural, hydrous sodium-potassium micas.

In Table 4, the lattice parameters of the dehydroxylated and the corresponding hydrous mica phases are com-

TABLE 4. Lattice parameters of hydrous dioctahedral micas and their dehydroxylated equivalents

	a (Å)	b (Å)	c (Å)	β (°)
		Sodium micas		
Paragonite-2M$_1$ (Chatterjee, 1974)	5.1304(10)	8.8927(15)	19.2698(28)	94.220(16)
Dehydroxylated paragonite-2M$_1$ (this paper)	5.244(8)	8.893(11)	19.463(5)	91.20(8)
		Potassium micas		
Muscovite-2M$_1$ (Chatterjee and Johannes, 1974)	5.1871(8)	8.9927(12)	20.1490(22)	95.780(10)
Dehydroxylated muscovite-2M$_1$ (this paper)	5.225(4)	9.163(5)	20.275(5)	95.776(26)
		Rubidium micas		
Rb analogue of muscovite-2M$_1$ (Voncken et al., 1987)	5.215(3)	9.059(5)	20.59(1)	96.540(3)
Anhydrous rubidium mica (this paper)	5.243(4)	9.198(10)	20.764(6)	95.98(4)

Note: The lattice parameters for the water-free micas are from Table 2 of this paper. For the dehydroxylated muscovite, similar data have been published by Udagawa et al. (1974), Vedder and Wilkins (1969), and Eberhart (1963).

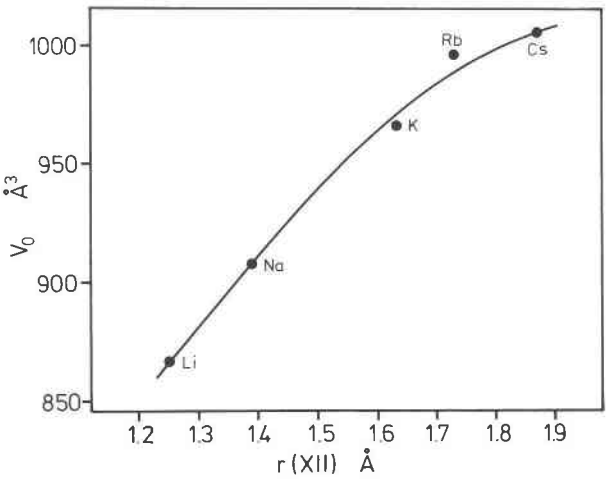

Fig. 9. Plot of the cell volume against the radius of the interlayer cation for the alkali micas.

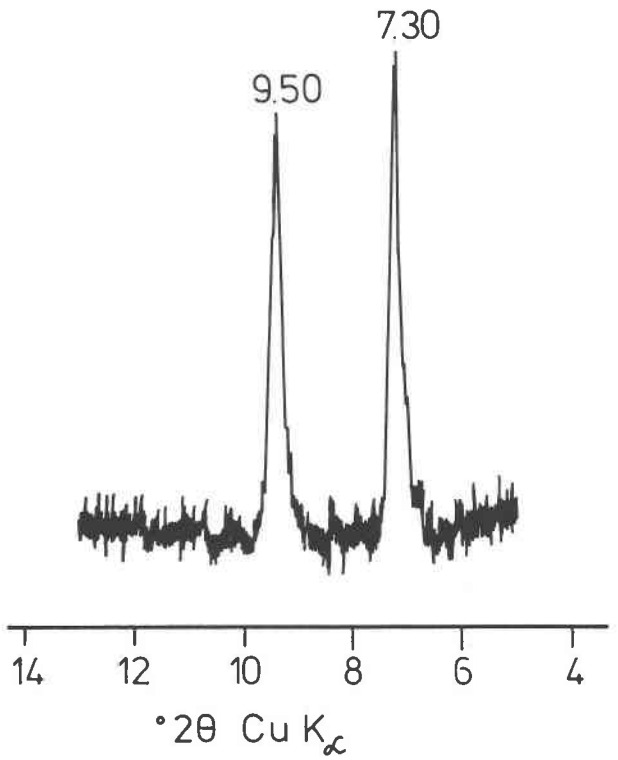

Fig. 10. Portion of the X-ray diffraction pattern of partially expanded lithium mica.

pared. The magnitudes of *a, b,* and *c* apparently increase during dehydroxylation of the sodium, potassium and rubidium micas. Only the change in the value of *b* of paragonite seems to be insignificant. At first sight, this is surprising, because the decrease in the coordination number of Al from 6 in the octahedral sheet of a mica to 5 in the dehydroxylated phase and the short Al-O distances in the latter structure (Udagawa et al., 1974) favor a decrease in the lattice parameters during dehydroxylation. In addition, the orientation of the O-H bond in dioctahedral micas points to repulsive forces between the proton and the interlayer cation (Bailey, 1984). Removal of the proton should therefore cause a contraction of the structure. The reason for the observed expansion of the mica structure during dehydroxylation is probably the disappearance of H bridges. On the basis of the fine structure of the OH valence vibration, Langer et al. (1981) postulated the existence of trifurcate H bridges in the structures of muscovite and paragonite. Because the H bridges have components in all three crystallographic directions, their disappearance during dehydroxylation could explain the increase in *a, b,* and *c.*

Geological applications

The geologically most important result of this study is the difference in the coordination of small and large interlayer cations in micas. In paragonite, strong repulsive forces across the interlayer seem to be present, whereas no such effect exists in muscovite. The corresponding structural differences explain the existence of a miscibility gap between paragonite and muscovite. According to Fujii (1966), the basal spacing of muscovite-paragonite solid solutions as a function of the Na-K ratio is not a straight line, but is strongly sigmoidal, a relation that is in agreement with the structural model outlined in this paper. The existence of repulsive forces across the interlayer of paragonite weakens the chemical bonding of sodium ions in the mica structure. This causes the preferential uptake of K^+ compared to Na^+ in micas and clay minerals of related structure, which ultimately leads to the enrichment of Na^+ over K^+ in sea water (e.g., Krauskopf, 1967). The thermodynamic stability field of paragonite is much smaller than that of muscovite. Paragonite decomposes to feldspar and corundum at much lower temperatures than muscovite (Chatterjee, 1970; Chatterjee and Johannes, 1974). In addition, the assemblage paragonite + quartz has a lower thermal stability limit (Chatterjee, 1973), whereas muscovite + quartz is stable under sedimentary *P, T* conditions. It is possible that these differences are partially caused by the relative destabilization of the paragonite structure by repulsion across the interlayer.

Conclusions

Ion-exchange reactions between micas and salt melts can be used to introduce many different cations into the interlayer of a mica. Very unusual phases can be obtained, such as micas with the extremely small Li^+ ion in the distorted 12-fold–coordinated site of the interlayer. The variation in the lattice parameters with the size of the interlayer cation indicates the existence of repulsive forces across the interlayer of micas containing small interlayer cations such as Na^+ or Li^+. The appearance of repulsive forces in the structure when the size of the in-

terlayer cation is less than that of a critical value may be important for the understanding of many features of the crystal chemistry of micas, e.g., the miscibility gap between paragonite and muscovite and the preferential uptake of K in micas and structurally related clay minerals.

Acknowledgments

The author thanks E. Althaus for the permission to conduct this study in the laboratories of the Mineralogical Institute of the University of Karlsruhe, Federal Republic of Germany. My colleague Laurinda Chamberlin (Caltech) kindly corrected the English of the original manuscript. The quality of the manuscript was improved by reviews and critical comments by Niranjan D. Chatterjee, Petr Černý, and Michael F. Hochella.

References cited

Bailey, S.W. (1984) Crystal chemistry of the true micas. Mineralogical Society of America Reviews in Mineralogy, 13, 13–60.

Chatterjee, N.D. (1970) Synthesis and upper stability of paragonite. Contributions to Mineralogy and Petrology, 27,244–257.

Chatterjee, N.D. (1973) Low-temperature compatibility relations of the assemblage quartz-paragonite and the thermodynamic status of the phase rectorite. Contributions to Mineralogy and Petrology, 42, 259–271.

Chatterjee, N.D. (1974) X-ray powder pattern and molar volume of synthetic 2M paragonite: A refinement. Contributions to Mineralogy and Petrology, 43, 25–28.

Chatterjee, N.D., and Johannes, W. (1974) Thermal stability and standard thermodynamic properties of synthetic $2M_1$-muscovite, $KAl_2[AlSi_3O_{10}(OH)_2]$. Contributions to Mineralogy and Petrology, 48, 89–114.

Cotton, F.A., and Wilkinson, G. (1980) Advanced inorganic chemistry (4th edition), Wiley, New York.

Eberhart, P.J. (1963) Étude des transformations du mica muscovite par chauffage entre 700 and 1200 °C. Bulletin de la Société Française de Minéralogie et de Cristallographie, 86, 213–251.

Flux, S., and Chatterjee, N.D. (1986) Experimental reversal of the Na-K exchange reaction between muscovite-paragonite crystalline solutions and 2 molal aqueous (Na,K)Cl fluid. Journal of Petrology, 27, 665–676.

Franz, G., and Althaus, E. (1976) Experimental investigation on the formation of solid solutions in sodium-aluminium-magnesium micas. Neues Jahrbuch für Mineralogie Abhandlungen, 126,233–253.

Fujii, T. (1966) Muscovite-paragonite equilibria, 180 p. Ph.D. thesis, Harvard University, Cambridge, Massachusetts.

Gmelin, L. (1927) Gmelins Handbuch der Anorganischen Chemie, System 20, Lithium (8th edition), p. 122. Verlag Chemie, Berlin.

Gmelin, L. (1957) Gmelins Handbuch der Anorganischen Chemie, System 28, Calcium, Teil B (8th edition), p. 445. Verlag Chemie, Weinheim.

Iiyama, J.T. (1964) Étude des réactions d'échange d'ions Na-K dans la série muscovite-paragonite. Bulletin de la Société Française de Minéralogie et de Cristallographie, 87, 532–541.

Keppler, H. (1988) Ion exchange reactions between micas and salt melts. Terra Cognita, 8, 67.

Krauskopf, K.B. (1967) Introduction to geochemistry, 721 p. McGraw Hill, New York.

Krausz, K. (1974) Potassium-barium exchange in phlogopite. Canadian Mineralogist, 12, 394–398.

Langer, K., Chatterjee, N.P., and Abraham, K. (1981) Infrared studies of some synthetic and natural $2M_1$ dioctahedral micas. Neues Jahrbuch für Mineralogie Abhandlungen, 142, 91–110.

Lin, C., and Bailey, S.W. (1984) The crystal structure of paragonite-$2M_1$. American Mineralogist, 69, 122–127.

McCauley, J.W., and Newnham, R.E. (1971) Origin and prediction of ditrigonal distortions in micas. American Mineralogist, 56, 1626–1638.

Radoslovich, E.W., and Norrish, K. (1962) The cell dimensions and symmetry of layer-lattice silicates. I. Some structural considerations. American Mineralogist, 47, 599–616.

Scott, A.D., and Smith, S.J. (1966) Susceptibility of interlayer potassium in micas to exchange with sodium. Clays and Clay Minerals, 14, 69–81.

Shannon, R.D. (1976) Revised effective ionic radii and systematic studies of interatomic distances in halides and chalcogenides. Acta Crystallographica, A 32, 751–767.

Udagawa, S., Urabe, K., and Hasu, H. (1974) The crystal structure of muscovite dehydroxylate. The Journal of the Japanese Association of Mineralogists, Petrologists, and Economic Geologists, 69, 381–389 (in Japanese).

Vedder, W., and Wilkins, R.W.T. (1969) Dehydroxylation and rehydroxylation, oxidation and reduction of micas. American Mineralogist, 54, 482–509.

Voncken, J.H.L., van der Eerden, A.M.J., and Jansen, J.B.H. (1987) Synthesis of a Rb analogue of $2M_1$ muscovite. American Mineralogist, 72, 551–554.

White, J.L. (1954) Reactions of molten salts with layer lattice silicates. Nature, 174, 799–800.

Manuscript received July 12, 1989
Manuscript accepted February 6, 1990

Appendix 1. X-ray powder-diffraction data for anhydrous micas

The lattice parameters of all micas mentioned in this appendix are given in Table 3. The following abbreviations are used in the appendix tables (Tables A1–A7): a = asymmetrical reflection, dff = diffuse reflection, * = reflection used for refinement of lattice constants.

Table A1. X-ray powder-diffraction data for lithium mica $LiAl_2[AlSi_3O_{10}O]$

hkl	I/I_0	d_{obs} (Å)	d_{calc} (Å)	
002	11	9.339	9.357	*
004	14	4.683	4.679	*
110	28	4.491	4.509	*
$\bar{1}11$	38	4.411	4.391	*
021	48	4.314	4.298	*
$\bar{1}12$	6	4.077	4.074	*
022	7	3.981	3.994	*
$\bar{1}13$	6	3.667	3.668	*
$\bar{1}14$	12	3.256	3.259	*
006	100	3.120	3.119	*

Note: The sample contains considerable amounts of decomposition products. Therefore, only the reflections are listed that can be unambiguously assigned to the mica.

TABLE A2. X-ray powder-diffraction data for sodium mica (dehydroxylated paragonite) $NaAl_2[AlSi_3O_{10}O]$

hkl	I/I_0	d_{obs} (Å)	d_{calc} (Å)	
002	16	9.707	9.729	*
004	19	4.864	4.865	*
110	19	4.509	4.516	*
$\bar{1}11$	23	4.411	4.417	*
$\bar{1}12$	3	4.131	4.125	*
022	7	4.035	4.044	*
$\bar{1}13$	7	3.739	3.738	*
023	2	3.648	3.667	*
$\bar{1}14$	24	3.331	3.340	*
006	100	3.241	3.243	*
025	9	2.954	2.928	*
115	9	2.923	2.922	*
$\bar{1}16$	2	2.661	2.657	*
$\bar{1}30$	18	2.600	2.580	
131	6	2.556	2.555	*
202	9	2.523	2.518	
008	6	2.431	2.432	*
$\bar{1}17$	2	2.380	2.387	dff
220	4	2.256	2.258	dff
0,0,10	9	1.945	1.946	*
0,0,12	2	1.622	1.622	*

Note: Several weak and broad reflections at higher angles.

TABLE A3. X-ray powder-diffraction data for potassium mica (dehydroxylated muscovite) $KAl_2[AlSi_3O_{10}O]$

hkl	I/I_0	d_{obs} (Å)	d_{calc} (Å)	
002	13	10.071	10.068	*
004	23	5.039	5.043	*
$\bar{1}11$	43	4.511	4.497	*
111	2	4.326	4.332	*
112	2	3.988	3.997	
$\bar{1}13$	7	3.914	3.914	*
023	8	3.789	3.786	
$\bar{1}14$	8	3.524	3.523	*
006	100	3.361	3.362	*
114	10	3.228	3.229	*
025	7	3.032	3.028	*
115	9	2.887	2.887	*
$\bar{1}16$	5	2.819	2.819	*
131	37	2.595	2.594	*
008	24	2.523	2.521	*
133	7	2.412	2.411	*
$\bar{2}21$	13	2.265	2.269	
0,0,10	25	2.017	2.017	*
$\bar{1}37$	6	1.994	1.995	*
$\bar{2}$,0,10	7	1.677	1.677	*
139	7	1.666	1.665	*
156	8	1.516	1.517	
315			1.516	

TABLE A4. X-ray powder-diffraction data for rubidium mica $RbAl_2[AlSi_3O_{10}O]$

hkl	I/I_0	d_{obs} (Å)	d_{calc} (Å)	
002	1	10.258	10.326	
004	2	5.143	5.163	
$\bar{1}11$	12	4.529	4.517	*
111	7	4.343	4.349	*
022	4	4.146	4.201	dff
112	7	4.020	4.021	*
$\bar{1}13$	18	3.958	3.956	*
023	20	3.826	3.824	*
113	4	3.642	3.640	
$\bar{1}14$	11	3.569	3.572	*
006	27	3.440	3.442	*
024	12	3.400	3.434	dff
114	12	3.265	3.264	*
025	10	3.072	3.073	*
115	14	2.924	2.925	*
$\bar{1}16$	7	2.870	2.870	*
026	8	2.758	2.756	
008	100	2.586	2.581	
027	5	2.484	2.483	
$\bar{1}18$	5	2.336	2.336	
$\bar{2}21$	15	2.277	2.277	
222	21	2.174	2.175	
0,0,10	29	2.065	2.065	*
$\bar{1}37$	7	2.023	2.022	
206	5	1.986	1.981	
139	7	1.689	1.689	dff
314	17	1.574	1.574	dff
156	17	1.527	1.528	dff

TABLE A5. X-ray powder-diffraction data for cesium mica $CsAl_2[AlSi_3O_{10}O]$

hkl	I/I_0	d_{obs} (Å)	d_{calc} (Å)	
002	25	10.782	10.749	*
004	8	5.369	5.374	*
$\bar{1}11$	8	4.527	4.535	*
111	12	4.381	4.379	*
$\bar{1}12$	9	4.334	4.329	dff
022	5	4.187	4.237	
112	16	4.064	4.069	*
$\bar{1}13$	21	4.006	4.003	*
023	25	3.878	3.877	*
$\bar{1}14$	22	3.633	3.632	*
006	4	3.579	3.583	*
024	18	3.485	3.499	
114	12	3.335	3.336	*
115	9	3.003	3.000	*
008	100	2.687	2.687	*
131	41	2.612	2.615	
027	7	2.554	2.556	
$\bar{2}21$	13	2.288	2.285	
$\bar{2}23$	23	2.228	2.226	
0,0,10	38	2.148	2.150	
$\bar{1}37$	8	2.059	2.058	
206	4	2.023	2.021	
0,0,12	6	1.791	1.791	dff
240	24	1.730	1.730	dff
0,2,12	7	1.670	1.670	dff
$\bar{2}$,0,12	4	1.554	1.552	dff
331	18	1.524	1.523	dff

TABLE A6. X-ray powder-diffraction data for thallium mica $TlAl_2[AlSi_3O_{10}O]$

hkl	I/I_0	d_{obs} (Å)	d_{calc} (Å)	
002	100	10.282	10.305	*
004	27	5.143	5.153	*
111	35	4.345	4.342	*
$\bar{1}12$	12	4.303	4.290	dff
112	39	4.020	4.015	*
$\bar{1}13$	52	3.943	3.947	*
023	55	3.814	3.816	*
113	21	3.635	3.634	*
$\bar{1}14$	40	3.563	3.563	*
006	18	3.422	3.435	
024			3.427	
$\bar{1}15$	25	3.207	3.194	
025	35	3.068	3.066	*
115	34	2.919	2.921	*
$\bar{1}16$	27	2.862	2.863	*
008	100	2.574	2.576	dff
027	20	2.481	2.478	dff
$\bar{1}18$	9	2.328	2.331	
041	23	2.278	2.280	
042	12	2.236	2.239	
204			2.233	
044	13	2.097	2.096	
0,0,10	38	2.061	2.061	*
$\bar{1}37$	10	2.020	2.017	
$\bar{1}$,1,10	6	1.948	1.943	

Note: The sample contained some unreacted starting material (dehydroxylated paragonite). Therefore, it is possible that some weak reflections of the thallium mica could not be observed because of the overlap with strong reflections of dehydroxylated paragonite.

TABLE A7. X-ray powder-diffraction data for calcium mica $Ca_{0.5}\square_{0.5}Al_2[AlSi_3O_{10}O]$

hkl	I/I_0	d_{obs} (Å)	d_{calc} (Å)	
$\bar{1}11$	13	4.435	4.427	*
022	13	4.035	4.044	*
$\bar{1}13$	72	3.739	3.753	*
023	13	3.642	3.668	dff
113			3.667	
$\bar{1}14$	26	3.356	3.354	*
006	100	3.214	3.245	a
025	10	2.948	2.929	dff
$\bar{1}31$	20	2.566	2.563	*
202	13	2.516	2.516	*
027	5	2.359	2.358	*
041	6	2.207	2.208	*
1,1,10	7	1.773	1.772	*

Note: Some very weak and diffuse reflections are not listed.